

# SINGLE-ANCHOR UWB LOCALIZATION USING CHANNEL IMPULSE RESPONSE DISTRIBUTIONS

Sitian Li\*      Alexios Balatsoukas-Stimming<sup>†</sup>      Andreas Burg\*

\* Telecommunication Circuits Laboratory, École polytechnique fédérale de Lausanne, Switzerland  
<sup>†</sup> Eindhoven University of Technology, The Netherlands

## ABSTRACT

Ultra-wideband (UWB) devices are widely used in indoor localization scenarios. Single-anchor UWB localization shows advantages because of its simple system setup compared to conventional two-way ranging (TWR) and trilateration localization methods. In this work, we focus on single-anchor UWB localization methods that learn statistical features of the channel impulse response (CIR) in different location areas using a Gaussian mixture model (GMM). We show that by learning the joint distributions of the amplitudes of different delay components, we achieve a more accurate location estimate compared to considering each delay bin independently. Moreover, we develop a similarity metric between sets of CIRs. With this set-based similarity metric, we can further improve the estimation performance, compared to treating each snapshot separately. We showcase the advantages of the proposed methods in multiple application scenarios.

**Index Terms**— Single-anchor localization, channel impulse response, ultra-wideband, Gaussian mixture model

## 1. INTRODUCTION

Indoor localization using wireless communications signals has a wide range of applications, such as asset tracking, occupancy analytics, and navigation. Due to its low power consumption, short pulse duration, and robustness against multipath fading, ultra-wideband (UWB) has become a popular indoor localization method [1]. The IEEE 802.15.4a-2007 standard [2] first proposed two-way ranging (TWR), which enables measuring the time of the signal transmission between two devices, which are usually referred to as the tag and the anchor, in the absence of clock synchronization, in order to calculate the distance between the anchor and the tag. To estimate the location, a TWR system consisting of at least three anchors at known positions is required. The location of the tag is estimated by the distance between the tag and the anchors using trilateration. However, TWR still relies on devices with extremely stable clocks [3, 4] and requires line-of-sight (LOS) transmission between the tag and anchors to operate well [5].

Single-anchor UWB localization methods have attracted significant attention recently. Instead of regarding the multipath channel as a problem for positioning as in TWR, single-anchor methods regard reflected transmission paths as virtual anchors [6, 7]. A very important channel characteristic, namely the channel impulse response (CIR), is a vector containing multiple delay bins calculated by the receiver. Each delay bin is a superposition of multiple transmission paths with different delays in the physical environment. For each

possible position of the anchor, the expected CIR from the anchor and virtual anchors are calculated and compared with the measured CIR. However, in order to know the accurate position of the anchors to localize the tag, the structure of the room (floor plan) needs to be obtained. Furthermore, only a few reflection paths on the walls have been considered in the literature, and high-order reflections, diffraction or diffuse scattering are not considered, which limits the positioning accuracy.

Since it is almost impossible to have a closed-form expression of the CIR in a room with a complex structure, learning-based approaches have been proposed to identify reasonably accurate mappings between the CIR and the position of the tag. Several works train a localization model to take a CIR snapshot, the linear projection of a CIR onto a low dimensional space, and other features such as the received signal strength indicator (RSSI) as input to the model [8, 9, 10]. However, there are still drawbacks to training from individual CIR snapshots. First, due to the lack of synchronization between the tag and the anchor [11, 12, 13], the measured CIR is shifted randomly and is multiplied with an additional random phase term. Even if the tag is stable, the received CIRs can be different since there is always a residual offset after the packet detection. Second, since the resolution of UWB is not sufficient to retrieve and separate all reflected paths, a CIR snapshot is a low-dimensional representation of a high-dimensional physical environment. Hence, we potentially need more snapshots as additional information for a good location estimate.

Therefore, the work of [14] proposed to consider CIR statistics instead of individual realizations. One intuitive method to learn a statistic is to assume a Gaussian mixture model (GMM), which has been applied successfully to other wireless communication positioning methods such as finger-printing in WiFi localization [15]. In those methods, the room is first divided into several pre-defined areas (around  $0.01 \text{ m}^2$ ), a large number of CIRs are sampled in each area, and the distribution for each delay bin in the CIR in each area is recorded and modeled by a GMM. When a new CIR observation becomes available, a log-probability-based score is calculated for each reference area and the area with the highest score is the location estimate. The score is calculated by treating the delay bins in one CIR as independent variables. However, better performance can be expected when considering one CIR with multiple delay bins as a sample from a multi-variate distribution of the pre-defined areas. Moreover, when the pre-defined areas become larger, the true physical distribution becomes challenging to model with a limited number of Gaussian distributions, and it becomes difficult to distinguish between the pre-defined areas. In [14], majority voting is proposed, which considers the hard decisions from multiple CIR snapshots during movement in the same area and improves the estimation accuracy. Since multiple samples are needed for the majority voting, a joint decision on the

This research has been kindly supported by the Swiss National Science Foundation under Grant-ID 182621.

soft scores is expected to perform better than majority voting among individual hard decisions.

## Contributions

In this work, instead of assuming that CIR bins are independent, we use a multi-bin GMM-based joint distribution. Moreover, we consider multiple CIR snapshots as a new sample set and propose to define a joint decision-based similarity metric between the new sample set and the sample sets in reference areas. To localize a set of CIRs with the similarity metric, we introduce two estimation methods: One is to simply choose the candidate with the maximum similarity, and the other is to apply machine learning to obtain the mapping between vectors of similarity metrics and the location area of the samples. Single-anchor localization, on the one hand, relies on a rich set of multipaths to estimate the position, but on the other hand, can be sensitive to multipath component changes, which decreases the localization accuracy. We thus test the performance of several methods in different environments, whose layout complexity varies. Our methods improve the estimation accuracy by up to 40% compared to the methods proposed until now in the literature. We also explore the robustness of single-anchor localization against layout changes in the same room.

## 2. BACKGROUND

In this section, we first briefly introduce the CIR and how it is estimated in the UWB receiver. Then, the localization method from [14] is introduced as a baseline.

### 2.1. Channel Impulse Response (CIR)

The IEEE 802.15.4 UWB preamble sequences [2] have a perfect periodic auto-correlation, which in essence allows a coherent receiver to estimate the CIR between the transmitter and the receiver [16]. There is usually a distortion residual in the estimated CIR because of the non-synchronized transmitter and receiver. In the following, the estimated CIR is denoted by a complex-valued vector  $\mathbf{h}$ .

### 2.2. One-dimensional Gaussian Mixture Model (1D-GMM)

The localization method described in [14] is divided into two phases. In the offline learning phase, a large number of CIRs  $\mathbf{h}_c^t$  are measured from each pre-defined area  $c \in \mathcal{C}$ , where  $t$  is the snapshot index and  $\mathcal{C}$  denotes the set of reference area indices. Each  $\mathbf{h}_c^t$  is a vector whose entries represent delay bins of the CIR. For each delay bin  $m$  and area  $c$ , the amplitude of  $\mathbf{h}_c^t[m]$  for all snapshot indices  $t$  is fitted using a GMM whose probability density function (PDF) is denoted by  $g_c^m$ . In the online phase, the estimated area  $\hat{l}^t$  for a new CIR sample  $\mathbf{h}^t$  is given by

$$\hat{l}^t = \arg \max_{c \in \mathcal{C}} \sum_{m=0}^{M-1} \log g_c^m(|\mathbf{h}^t[m]|), \quad (1)$$

where  $M$  is the number of considered delay bins.

## 3. PROPOSED METHODS

We first propose our multi-dimensional GMM method. Then, we describe the position estimation method using the similarity metric.

### 3.1. Multi-dimensional Gaussian Mixture Model (MD-GMM)

Note that (1) treats the magnitudes  $|\mathbf{h}^t[m]|$  at multiple delay bins  $m$  as independent variables. However, because of the potentially complex reflection environment, the adjacent delay bins can be impacted

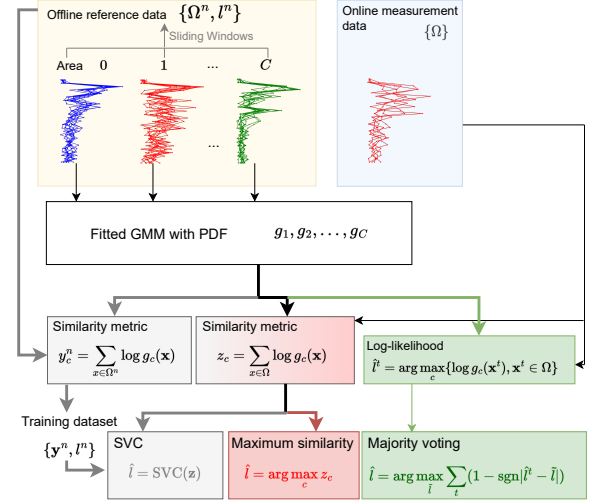


**Fig. 1.** Block Diagram of MD-GMM (green), MD-GMM-MaxSim (red) and MD-GMM-SVC (gray). The yellow box denotes reference CIR set, the blue box denotes one sample set during online measurement phase. The white box is the GMM fitting block that is shared by all methods.

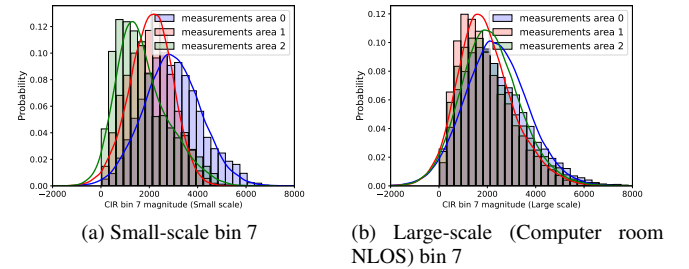


**Fig. 2.** Marginal CIR magnitude histograms (rectangles) and fitted MD-GMM marginal distributions (solid lines) in different areas

by the same delay path and are thus generally correlated. For this reason, we propose to consider each  $|\mathbf{h}^t|$  as a multi-variate random variable and to fit a  $M$ -dimensional GMM whose PDF is  $g_c$  for each area  $c$  in the offline training phase, as shown by the white box in Fig. 1. In the online test phase, we measure the log-probability of  $\mathbf{h}^t$  for each  $t$  being sampled from all the individual reference GMMs. The estimated area  $\hat{l}^t$  for  $\mathbf{h}^t$  is then defined as

$$\hat{l}^t = \arg \max_{c \in \mathcal{C}} \log g_c(|\mathbf{h}^t|). \quad (2)$$

Intuitively, by inspecting all delay bins of the CIR jointly, the performance should benefit from considering the multi-variate CIR distribution. To further improve the accuracy, we then apply a majority vote as in [14] according to

$$\hat{l} = \arg \max_{\tilde{l} \in \mathcal{C}} \sum_{t=1}^T (1 - \text{sgn}(|\hat{l}^t - \tilde{l}|)), \quad (3)$$

for a set of consecutive samples  $|\mathbf{h}^t|$ , denoted by  $\Omega$ , where  $\text{sgn}(\cdot)$  is the sign function and  $T$  is the number of snapshots.

### 3.2. Similarity Metric based on MD-GMM

Even though the performance can be improved by majority voting from multiple snapshots, there are two drawbacks to the previously

described log-probability-based methods: First, we observed that when the distribution of the physical channel is complicated, the PDFs become difficult to distinguish between areas, especially when the area in each location is large (e.g.,  $1 \text{ m}^2$ ) and the environment has many obstacles. As shown in Fig. 2, we plot the marginal CIR distributions on delay bin 7. For the non-line-of-sight (NLOS) case, the distributions and the fitted GMMs of different areas can be more similar compared to the small-scale case. Second, the majority voting based on hard decisions can be improved by a joint soft decision among multiple snapshots. Thus we propose to regard multiple snapshots as samples from a new distribution  $\Omega$ , and estimate the location by a similarity metric between the distribution of a new sample set and the distributions of the reference sample sets in different areas.

The estimation based on the log-probability with the GMM is in fact closely related to searching for the reference area  $\hat{l}$  whose GMM with the PDF  $g_l$  has the smallest Kullback-Leibler divergence (KLD) with the sampled set  $\Omega$ . More specifically, suppose that the PDF of  $\Omega$  is  $f_\Omega(\mathbf{x})$ . Then we have

$$\hat{l} = \arg \min_{c \in \mathcal{C}} \text{KLD}(f_\Omega \| g_c) = \arg \min_{c \in \mathcal{C}} \int f_\Omega(\mathbf{x}) \log \frac{f_\Omega(\mathbf{x})}{g_c(\mathbf{x})} d\mathbf{x} \quad (4)$$

$$= \arg \max_{c \in \mathcal{C}} \int f_\Omega(\mathbf{x}) \log g_c(\mathbf{x}) d\mathbf{x} \quad (5)$$

$$\approx \arg \max_{c \in \mathcal{C}} \sum_{t=1}^T \log g_c(\mathbf{x}^t), \quad (6)$$

where  $\mathbf{x}^t, t = 1 \dots T$  are i.i.d. sampled from the distribution  $f(\mathbf{x})$ . Eq. (6) becomes an equality when  $T \rightarrow \infty$ . Inspired by this observation, we define

$$z_c = \sum_{t=1}^T \log g_c(|\mathbf{h}^t|) \quad (7)$$

as the similarity metric between  $\Omega$  and  $g_c$  and we pick the class  $c$  with the largest similarity measure as the location estimate. We refer to this method illustrated by red boxes in Fig. 1 as MD-GMM-MaxSim.

The similarity metric is defined based on the assumption that all samples from  $\Omega$  are i.i.d. distributed, which is not true since the samples are typically recorded over a short time window. As an alternative method, we propose to learn the mapping between the location area and the similarity metric vector  $\mathbf{z}$ . We call this method MD-GMM-SVC and we use reference datasets for training as well as a support vector classification (SVC) as shown with gray boxes in Fig. 1. Compared to other methods, MD-GMM-SVC has an additional training step after the joint GMMs are obtained. The reference dataset is sliced into sliding windows indexed by  $n$  of  $T$  snapshots each, which creates sample sets of  $|\mathbf{h}|$ , denoted by  $\Omega^n$ , with corresponding labels  $l^n$  indicating the area in which the sample sets are collected. We compute the similarity metric as in (7). The set of similarity metrics  $\mathbf{y}^n$  together with the labels  $l^n$  are used to learn the mapping between the similarity metric and the location area using SVC. In the online test phase, for a set of new observations  $\Omega$ , we first measure the similarity metric  $\mathbf{z}$ , and then use the trained SVC model to decide the location area  $\hat{l}$ .

## 4. EXPERIMENTAL STUDY

In this section, we evaluate the performance of the three methods described in Section 3 in different scenarios with the method in Section 2.2 as the baseline. For each scenario, we divide the considered area into 12 sub-areas, and each has an area label. We localize the transmitter by deciding in which area the transmitter is positioned.

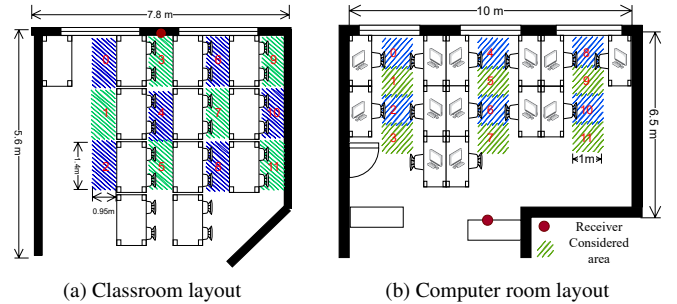
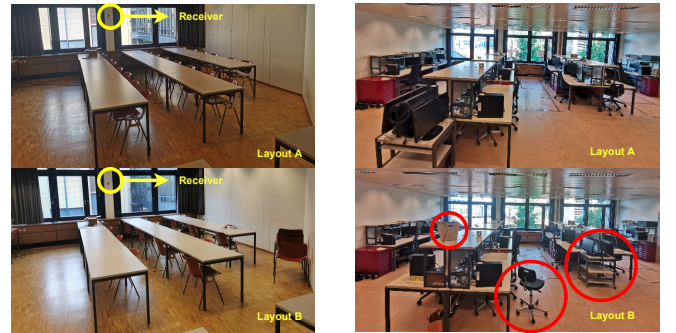


Fig. 3. Layout of the large-scale setups



(a) Original classroom layout (top) and layout with moved chairs (bottom).

(b) Original computer room layout (top) and layout with moved objects marked with red circles (bottom), the receiver is next to the camera.

Fig. 4. Layout changes in the large-scale setups

### 4.1. Experiment Setup

We use the same UWB chip DW1000 [17] for both the transmitter and the receiver. The transmitter is moving in the considered areas, sending packets in UWB channel 5 with an interval of 0.02 s. The receiver records and stores the first 50 bins in the CIR. Note that in DW1000, the CIR bins are interpolated such that each bin represents half a period of the 499.2 MHz fundamental frequency [16], so we filter the CIR in the frequency domain and down-sample the CIR such that we only need to consider 25 bins after filtering. We considered the three following measurement scenarios.

#### 4.1.1. Small-scale scenario

First, we test in a small-scale scenario, where the transmitter is attached to a two-axis computer numerical control (CNC) machine and the receiver is located at a distance of 3 m. The CNC is programmed to move the transmitter within the pre-defined areas of size 8.5 cm by 8.5 cm, which also corresponds to the scale of the setup in [14].

#### 4.1.2. Large-scale scenario (classroom)

We also conduct measurements in a classroom of size  $5.6 \text{ m} \times 7.8 \text{ m}$ . The receiver is located 2 m above the floor and the transmitter is carried by a walking person, in positions in which people typically hold their phones. The receiver is most of the time in the LOS of the transmitter, except for the moment when the carrying person is blocking the LOS depending on the walking direction. The considered area consists of 12 sub-areas of size  $1.4 \text{ m} \times 0.95 \text{ m}$  as shown in Fig. 3a. In order to test the robustness of the different methods against environment changes, we move the chairs in the classroom as shown in

		Small-scale scenario	Classroom A1→A2	Classroom A1→B	Computer room (LOS) A1→A2	Computer room (LOS) A1→B	Computer room (NLOS) A1→A2	Computer room (NLOS) A1→B
<b>1D-GMM [14]</b>	1 snapshot	61.1%	41.1%	33.8%	47.1%	41.4%	28.1%	26.2%
	MV100	77.2%	67.5%	56.6%	87.9%	76.5%	56.5%	50.6%
<b>MD-GMM</b>	1 snapshot	92.5%	59.8%	49.4%	56.6%	44.9%	37.0%	33.8%
	MV100	99.4%	99.9%	94.8%	97.7%	85.7%	86.2%	81.2%
<b>MD-GMM -MaxSim</b>	100 snapshots	99.8%	100.0%	94.9%	98.5%	88.9%	92.5%	90.1%
<b>MD-GMM -SVC</b>	100 snapshots	99.7%	99.9%	95.7%	99.4%	89.8%	95.0%	91.9%

**Table 1.** Localization accuracy with different methods in different scenarios. Majority voting among 100 snapshots is denoted by MV100.

Fig. 4a to create a second room layout and collect two datasets with two different room layouts.

#### 4.1.3. Large-scale scenario (computer room)

We also collect data in a more complex environment that is equipped with desks, shelves, and computers as shown in Fig. 3b of size  $6.5\text{m} \times 10\text{m}$ . The sub-areas are  $1\text{m} \times 1\text{m}$ . The receiver is located 1.8m above the floor. The computer room allows us to test both LOS and NLOS scenarios. If the transmitter is held in hand, the LOS is most of the time blocked by shelves and computers. If the transmitter is held high up in the air, the LOS is guaranteed most of the time. Two datasets are collected with different layouts as shown in Fig. 4b.

#### 4.2. Data Collection

In the small-scale scenario, we test the performance with LOS and without environment changes. Both training and test sets contain 5500 snapshots. In the large-scale scenarios (classroom, computer room (LOS) and computer room (NLOS)), two datasets are collected for two different layouts and are denoted by set A and set B in each scenario. For the classroom, set A contains 5200 snapshots. The first 4000 snapshots are denoted as training set A1 and the last 1200 snapshots are denoted as test set A2. Set B contains 1200 snapshots with layout changes compared to set A for test. For the computer room case, we collect more data since the environment is more complicated. Set A contains 12000 samples. The first 10800 snapshots are denoted as training set A1 and the last 1200 snapshots are denoted as test set A2. Set B contains 1200 snapshots for test again with layout changes. We test the robustness against the room layout change by training with the samples in set A1, and testing with the samples in set A2 and set B in each scenario. For the 1D-GMM method and the MD-GMM method, majority voting is performed over 100 snapshots. For the similarity metric-based methods (MD-GMM-MaxSim and MD-GMM-SVC), each sample set contains 100 snapshots for a fair comparison.

#### 4.3. Offline Learning Parameters

In the offline phase, we use the variational Bayesian estimation of a Gaussian mixture function provided by the *scikit-learn* toolbox [18], with a maximum of 2 Gaussian components for 1D-GMM and 5 Gaussian components for MD-GMM, a maximum of  $10^4$  iterations, a convergence threshold of  $10^{-3}$  and a weight concentration prior of  $10^{-3}$ . We use the SVC supported by the same toolbox, with the radial basis function kernel and maximum iteration of  $10^4$ . The other parameters are as default in the toolbox version 1.0.2.

#### 4.4. Results

The localization accuracy is shown in Table 1. Both GMM-based methods benefit from majority voting. The 1D-GMM shows good results in the small-scale environment with an accuracy of 77.2% with majority voting. However, when the considered areas become larger, as in the classroom and the computer room, MD-GMM shows a considerably better performance than 1D-GMM. After majority voting, the MD-GMM achieves up to 99.9% accuracy in the classroom setup, and is quite robust to room layout change with an accuracy of 94.8%. In more complicated environments in the computer room, with the LOS scenario, MD-GMM achieves an accuracy of 97.7% without layout changes, and 85.7% with layout changes. By introducing the similarity metric (MD-GMM-MaxSim and MD-GMM-SVM), the accuracy can be improved slightly by around 2%. However, in an environment with more NLOS cases, the similarity metric-based methods improve the accuracy by around 6% to 9% compared to MD-GMM with the majority voting. Even with layout changes, the MD-GMM-MaxSim still shows significant improvement and reaches an accuracy of 90.1% compared to the accuracy of 81.2% by MD-GMM. The SVC-based method shows slightly better performance compared to the MaxSim method in the NLOS scenario and the improvement is around 2%.

Regarding online estimation efficiency, estimation with 1D-GMM is about 16 times slower than with MD-GMM, since 1D-GMM needs to loop over each delay bin to calculate the probability, whereas MD-GMM considers all the delay bins jointly. Among all MD-GMM-based methods, using the SVC increases the run time by 20%, compared to the MD-GMM-MaxSim and the majority voting method.

### 5. CONCLUSIONS

In this paper, we showed that learning statistics of multiple CIRs leads to good performance in UWB single-anchor localization in environments with a rich amount of multipath. By properly combining the information obtained from multiple CIR delay bins, the localization accuracy shows significant improvement by up to 30% compared to considering each delay bin separately as done until now in the literature in large-scale environments. Instead of combining multiple hard decisions based on the probability of snapshots in GMMs of reference areas, directly considering the snapshots as a sample set and comparing the similarity metric between the CIR set and the reference CIR sets performs better. Especially in rooms with complex layouts and many obstacles, the similarity metric-based methods can further improve the performance by up to 10% compared to the majority voting method.

## 6. REFERENCES

- [1] Zhu Xiao, YongQiang Hei, Quan Yu, and KeChu Yi, "A survey on impulse-radio UWB localization," *Science China Information Sciences*, vol. 53, no. 7, pp. 1322–1335, July.
- [2] "IEEE Standard for Information technology – Local and metropolitan area networks – Specific requirements – Part 15.4: Wireless Medium Access Control (MAC) and Physical Layer (PHY) Specifications for Low-Rate Wireless Personal Area Networks (WPANs): Amendment 1: Add Alternate PHYs," Tech. Rep., IEEE, ISBN: 9780738155845.
- [3] Konstantin Mikhaylov, Antti Tikanmaki, Juha Petajajarvi, Matti Hamalainen, and Ryuji Kohno, "On the selection of protocol and parameters for UWB-based wireless indoors localization," in *2016 10th International Symposium on Medical Information and Communication Technology (ISMICT)*. Mar., pp. 1–5, IEEE.
- [4] Juri Sidorenko, Volker Schatz, Norbert Scherer-Negenborn, Michael Arens, and Urs Hugentobler, "Decawave UWB clock drift correction and power self-calibration," *Sensors*, vol. 19, no. 13, pp. 2942, July.
- [5] Milad Heydariaan, Hessam Mohammadmoradi, and Omprakash Gnawali, "Toward standard non-line-of-sight benchmarking of ultra-wideband radio-based localization," in *2018 IEEE Workshop on Benchmarking Cyber-Physical Networks and Systems (CPSBench)*. Apr., pp. 19–24, IEEE.
- [6] Bernhard Großwindhager, Michael Rath, Josef Kulmer, Stefan Hinteregger, Mustafa Bakr, Carlo Alberto Boano, Klaus Witrals, and Kay Römer, "UWB-based single-anchor low-cost indoor localization system," in *Proceedings of the 15th ACM Conference on Embedded Network Sensor Systems*. Nov., pp. 1–2, ACM.
- [7] Bernhard Großwindhager, Michael Rath, Josef Kulmer, Mustafa S. Bakr, Carlo Alberto Boano, Klaus Witrals, and Kay Römer, "SALMA: UWB-based single-anchor localization system using multipath assistance," in *Proceedings of the 16th ACM Conference on Embedded Networked Sensor Systems*. Nov., pp. 132–144, ACM.
- [8] Soumya Prakash Rana, Maitreyee Dey, Hafeez Ur Siddiqui, Gianluigi Tiberi, Mohammad Ghavami, and Sandra Dudley, "UWB localization employing supervised learning method," in *2017 IEEE 17th International Conference on Ubiquitous Wireless Broadband (ICUWB)*. Sept., pp. 1–5, IEEE.
- [9] Sivanand Krishnan, Rochelle Xenia Mendoza Santos, Enhao Ranier Yap, and May Thu Zin, "Improving UWB based indoor positioning in industrial environments through machine learning," in *2018 15th International Conference on Control, Automation, Robotics and Vision (ICARCV)*. Nov., pp. 1484–1488, IEEE.
- [10] Yi-Min Lu, Jang-Ping Sheu, and Yung-Ching Kuo, "Deep learning for ultra-wideband indoor positioning," in *2021 IEEE 32nd Annual International Symposium on Personal, Indoor and Mobile Radio Communications (PIMRC)*. Sept., pp. 1260–1266, IEEE.
- [11] Jeroen D. Hol, Thomas B. Schon, and Fredrik Gustafsson, "Ultra-wideband calibration for indoor positioning," in *2010 IEEE International Conference on Ultra-Wideband*. Sept., pp. 1–4, IEEE.
- [12] Yiwei Zhuo, Hongzi Zhu, and Hua Xue, "Identifying a new non-linear CSI phase measurement error with commodity WiFi Devices," in *2016 IEEE 22nd International Conference on Parallel and Distributed Systems (ICPADS)*. Dec., pp. 72–79, IEEE.
- [13] Yaxiong Xie, Zhenjiang Li, and Mo Li, "Precise power delay profiling with commodity Wi-Fi," *IEEE Transactions on Mobile Computing*, vol. 18, no. 6, pp. 1342–1355, June.
- [14] Hessam Mohammadmoradi, Milad Heydariaan, Omprakash Gnawali, and Kyungki Kim, "UWB-based single-anchor indoor localization using reflected multipath components," in *2019 International Conference on Computing, Networking and Communications (ICNC)*. Feb., pp. 308–312, IEEE.
- [15] Shuyu Shi, Stephan Sigg, and Yusheng Ji, "Probabilistic fingerprinting based passive device-free localization from channel state information," in *2016 IEEE 83rd Vehicular Technology Conference (VTC Spring)*. May, pp. 1–5, IEEE.
- [16] Decawave, "DW1000 User manual," <http://www.qorvo.com/products/d/da007967>, visited 2022-10-04.
- [17] Decawave, "DW1000 Datasheet," <http://www.qorvo.com/products/d/da007946>, visited 2022-10-04.
- [18] F. Pedregosa, G. Varoquaux, A. Gramfort, V. Michel, B. Thirion, O. Grisel, M. Blondel, P. Prettenhofer, R. Weiss, V. Dubourg, J. Vanderplas, A. Passos, D. Cournapeau, M. Brucher, M. Perrot, and E. Duchesnay, "Scikit-learn: Machine learning in Python," *Journal of Machine Learning Research*, vol. 12, pp. 2825–2830, 2011.